

PDF hosted at the Radboud Repository of the Radboud University Nijmegen

The following full text is a preprint version which may differ from the publisher's version.

For additional information about this publication click this link.

<http://hdl.handle.net/2066/84209>

Please be advised that this information was generated on 2017-12-06 and may be subject to change.

PARSEC-SCALE BIPOLAR X-RAY SHOCKS PRODUCED BY POWERFUL JETS FROM THE NEUTRON STAR CIRCINUS X-1

P. H. SELL¹, S. HEINZ¹, D. E. CALVELO², V. TUDOSE^{3,4,5}, P. SOLERI⁶, R. P. FENDER², P. G. JONKER^{7,8,9}, N. S. SCHULZ¹⁰, W. N. BRANDT¹¹, M. A. NOWAK¹⁰, R. WIJNANDS¹², M. VAN DER KLIS¹², P. CASELLA²

Draft version August 5, 2010

ABSTRACT

We report the discovery of multi-scale X-ray jets from the accreting neutron star X-ray binary, Circinus X-1. The bipolar outflows show wide opening angles and are spatially coincident with the radio jets seen in new high-resolution radio images of the region. The morphology of the emission regions suggests that the jets from Circinus X-1 are running into a terminal shock with the interstellar medium, as is seen in powerful radio galaxies. This and other observations indicate that the jets have a wide opening angle, suggesting that the jets are either not very well collimated or precessing. We interpret the spectra from the shocks as cooled synchrotron emission and derive a cooling age of ~ 1600 yr. This allows us to constrain the jet power to be $3 \times 10^{35} \text{ erg s}^{-1} \lesssim P_{\text{jet}} \lesssim 2 \times 10^{37} \text{ erg s}^{-1}$, making this one of a few microquasars with a direct measurement of its jet power and the only known microquasar that exhibits stationary large-scale X-ray emission.

Subject headings: ISM: jets and outflows, X-rays: binaries, X-rays: individual (Circinus X-1)

1. INTRODUCTION

Circinus X-1 is an unusual X-ray binary (XRB). Stewart et al. (1993) first noticed that Circinus X-1 resides inside of a parsec-scale radio nebula inflated by curved jets. More-recent radio observations have observed jet emission on multiple scales (Tudose et al. 2008, and references therein). Additionally, at the peak of the 40+ year X-ray light curve (see Figure 1 of Parkinson et al. 2003), Fender et al. (2004) detected evidence of superluminal motion from ultra-relativistic jets within a few arcseconds of the XRB, which would make this the only known accreting neutron star with an ultra-relativistic jet. With its resolved, parsec-scale radio jets, Circinus X-1 has become an important stepping stone in our understanding of microquasars over the past few decades.

Circinus X-1 has been extensively studied at X-ray

¹ Department of Astronomy, University of Wisconsin-Madison, Madison, WI 53706, USA

² School of Physics and Astronomy, University of Southampton, Southampton SO17 1BJ, UK

³ Netherlands Institute for Radio Astronomy, Postbus 2, 7990 AA Dwingeloo, The Netherlands

⁴ Astronomical Institute of the Romanian Academy, Cutitul de Argint 5, RO-040557 Bucharest, Romania

⁵ Research Center for Atomic Physics and Astrophysics, Atomistilor 405, RO-077125 Bucharest, Romania

⁶ Kapteyn Astronomical Institute, University of Groningen, P.O. Box 800, 9700 AV Groningen, The Netherlands

⁷ SRON, Netherlands Institute for Space Research, Sorbonnelaan 2, 3584 CA, Utrecht, The Netherlands

⁸ Department of Astrophysics, IMAPP, Radboud University Nijmegen, P.O. Box 9010, NL-6500 GL Nijmegen, the Netherlands

⁹ Harvard-Smithsonian Center for Astrophysics, 60 Garden Street, Cambridge, MA 02138, USA

¹⁰ Kavli Institute for Astrophysics and Space Research, Massachusetts Institute of Technology, Cambridge, MA 02139, USA

¹¹ Department of Astronomy and Astrophysics, The Pennsylvania State University, 525 Davey Laboratory, University Park, PA 16802, USA

¹² Astronomical Institute Anton Pannekoek, University of Amsterdam, Science Park 904, 1098XH Amsterdam, The Netherlands

wavelengths. Type-I X-ray bursts, originally observed by Tennant et al. (1986) and seen again by Linares et al. (2010) during a recent flare, now firmly establish that the compact object is an accreting neutron star. Multiple *Chandra* gratings observations of the point source have revealed variable X-ray P-Cygni line profiles that were interpreted as high-velocity outflows (Brandt & Schulz 2000; Schulz & Brandt 2002). Iaria et al. (2008) have claimed possible detection of a highly-inclined precessing jet (similar to SS433, e.g., Lopez et al. 2006) through Doppler-shifted X-ray line emission. However, this interpretation is not unique as the emission is also consistent with simple orbital motion of the neutron star. Moreover, Schulz et al. (2008) also analyzed that particular data set and, with systematic uncertainties included, find no shifts. Finally, in the longest gratings observation of the point source (zero-order, 50 ks) taken in 2005, Heinz et al. (2007) discovered faint, diffuse X-ray emission roughly coincident with the arcminute-scale radio jets. However, the observation had insufficient signal-to-noise to constrain the nature of the emission spectroscopically. Similar diffuse emission was subsequently seen in a 50 ks HRC-I observation (Soleri et al. 2009), but no spectral information was available with this instrument.

In this Letter, we report on a follow-up deep *Chandra* imaging observation of the diffuse X-ray emission found by Heinz et al. (2007). We outline our observations in Section 2 and present an initial analysis of the emission in Section 3. Section 4 discusses the physical implications. Finally, we summarize our results in Section 5. Throughout this Letter, we assume a distance of 7.8 kpc (Jonker et al. 2007), which is in the middle of a wide range of distance estimates (4.1–11.8 kpc; Iaria et al. 2005).

2. OBSERVATIONS

We observed Circinus X-1 on the S3 chip of the Advanced CCD Imaging Spectrometer (ACIS) aboard the *Chandra X-ray Observatory* on 2009 May 1, in a contin-

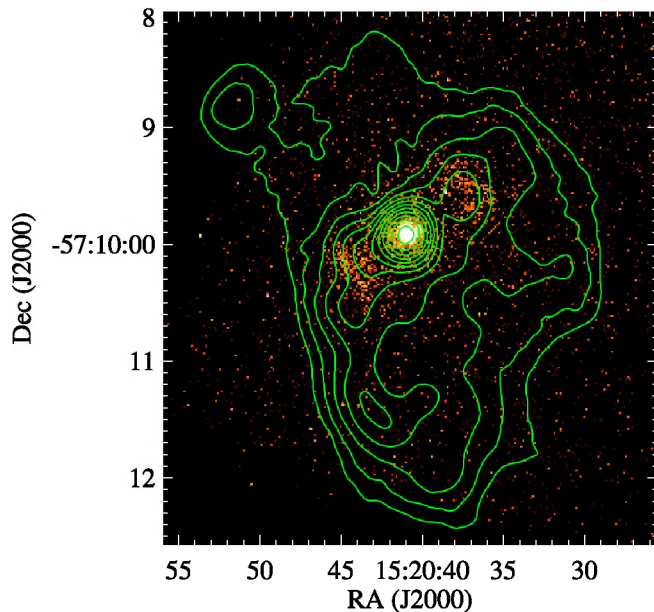


FIG. 1.— Reduced event file showing the point source and the bipolar “caps” created by the outflow. Overlaid are contours from the lower resolution radio image (logarithmically spaced from 1.9 to 25 mJy beam⁻¹; beam size: 18.''1 × 16.''5) from Tudose et al. (2006).

uous 99 ks exposure. Data were taken in timed exposure mode and telemetered in Faint mode. Data reduction and analysis were completed using CIAO and Sherpa versions 4.2, XSpec 12.5.1, and ACIS Extract version 2010-02-26 (AE; Broos et al. 2010). Compared to previous gratings and HRC-I observations, this observation proved about an order of magnitude more sensitive to diffuse flux not only because of the long exposure and the lack of gratings, but also because the contaminating emission from the point source was at an exceptionally low level (Section 3.1).

Radio comparison data were constructed from two separate observations. Standard calibrations using the Miriad software (Sault et al. 1995) were applied to both sets of observations. A low angular resolution radio image was derived from data taken on 2001 August 3 during an 11 hr run at 1.4 GHz with the Australia Telescope Compact Array (ATCA) in 1.5A array configuration. This observation and the resulting images were presented in Tudose et al. (2006) and are shown as contours in Figure 1.

A higher angular resolution radio image (Figure 2) was created from ~ 80 hr of observations spread from 2009 December 30 to 2010 January 8, using the ATCA-Compact Array Broadband Backend in 6A configuration at 5.5 GHz (D. E. Calvelo et al., in preparation).

3. ANALYSIS

The reduced event file of the X-ray observation is shown in Figure 1 with a contour overlay of the low-resolution radio image of the large-scale radio nebula of Circinus X-1. This image clearly shows the existence of two bright emission regions $\sim 30''$ from the point source.

In order to highlight the morphology of the diffuse emission closer to the point source and to allow detailed comparison with the high-resolution radio image, we created an exposure-corrected, background-subtracted im-

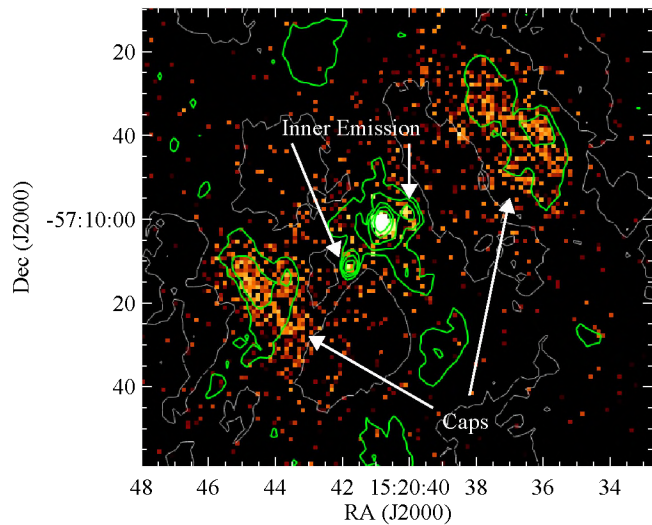


FIG. 2.— Exposure-corrected and azimuthally-smoothed, background-subtracted X-ray image. Overlaid are contours from the higher resolution radio image (levels: -1, 2, 4, 8, 16, 32 times rms noise of $\sim 6 \mu\text{Jy beam}^{-1}$; beam size: 3.''02 × 2.''21; D. E. Calvelo et al., in preparation). The point source, inner emission, and the X-ray caps described in Sections 3.1–3.3 are all evident here and well-matched to the radio contours.

age (Figure 2). Background surface brightness profiles were constructed by azimuthally averaging over nested partial annuli in the NE and SW quadrants (visually chosen to exclude the excess diffuse emission) and then subtracted from the exposure-corrected image.

Finally, we note that on the largest scales, we find roughly axisymmetric soft emission from what we interpret as the dust-scattering halo, centered on the binary, best visible in the adaptively-smoothed image in Figure 3. An in-depth discussion of the dust-scattering halo will be presented in a follow-up paper.

Image analysis and X-ray–radio comparisons are presented below, ordered from smaller to larger scales. All well-determined background/foreground point sources were masked and excluded from our analysis.

3.1. The Point Source

We caught Circinus X-1 at the lowest observed flux to date ($F_{0.5-8\text{keV}} \simeq 1 \times 10^{-11} \text{ erg cm}^{-2} \text{ s}^{-1}$). Even so, the source is still significantly piled up with a pileup fraction of $\sim 40\%$. We will present detailed model fits to the point source spectrum in a follow-up paper.

3.2. An Arcsecond Jet

Because the point source was so faint, the point spread function (PSF) from the XRB only dominates the inner $\sim 5''$. This enabled us to search for jet emission on scales of a fraction of a parsec, much smaller than what had been possible in Heinz et al. (2007) and Soleri et al. (2009). We found two sources within $\sim 15''$ of the point source, which are both evident in Figure 2:

1. In the W-NW direction (between position angles 0° and $+45^\circ$, measured counterclockwise from due W), we find a clear surface brightness enhancement separated from the XRB by $\sim 5''$ and extending out to $\sim 8''$. The emission appears to be *resolved* and

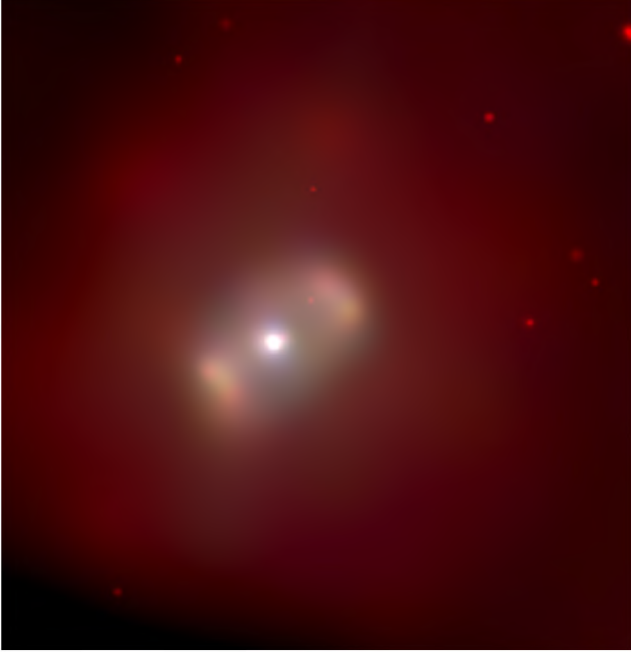


FIG. 3.— Adaptively smoothed three-color image $\sim 4/5 \times 4/5$ (red: 0.5–2.9 keV, green: 2.9–4.2 keV, and blue: 4.2–7.0 keV). The large-scale dust-scattering halo from the point source (red) and the hard wings of the PSF (blue) are clearly distinct in color from the cap emission. North is up and east is left.

is coincident with a source in the high-resolution radio image. No IR counterpart is found in either 24 μm MIPS GAL¹³ or 3.6–8 μm GLIMPSE¹⁴ *Spitzer* images. Given that the source is extended and aligned with the large-scale radio jet and with the X-ray caps reported below, we interpret this source as genuine jet emission.

2. In the SE direction (at position angle 230°), we detect a bright, *unresolved* point source at $\sim 13''$ from the XRB. This emission is coincident with a point-like radio source. It is spatially coincident with a very bright IR point source, with no optical counterpart detected in an archival 5 minute HST/WFPC I exposure.

From the FIRST (Faint Images of the Radio Sky at Twenty-Centimeters) $\log N$ – $\log S$, we estimate that the probability of finding a background radio point source of the same or larger flux within 13 arcseconds from Circinus X-1 is $\sim 1\%$. In addition, given the IR source density in the region, the likelihood of finding an IR background source with equal or larger flux coincident with the radio and X-ray point source within the MIPS PSF is also of order 1%. Neither scenario can be ruled out statistically. Thus, we cannot draw any conclusions about the nature of the SE point source without further observational evidence, e.g., from optical spectroscopy, variability, or proper motion.

A detailed PSF subtraction of the binary emission (complicated by effects of pileup) and spectral fits of

¹³ <http://mipsgal.ipac.caltech.edu/>

¹⁴ <http://www.astro.wisc.edu/sirtf/>

these sources are beyond the scope of this Letter and will be presented in a follow-up paper.

3.3. Extended Diffuse Emission: X-ray Caps

The most obvious features in Figures 1–3 are the two diffuse emission regions between $\sim 20''$ and $50''$ from Circinus X-1 in the NW and SE directions. The positions of both regions are consistent with the diffuse emission tentatively reported in Heinz et al. (2007) and Soleri et al. (2009). Based on their morphological appearance (NW cap appears slightly concave) and their placement away from the binary along the jet axis, we will refer to both regions as “caps” throughout the rest of this Letter. However, the geometry of these regions could be complicated by projection effects, and other interpretations are possible.

The caps have distinctly different X-ray colors from both the much redder large-scale diffuse background (dominated by the dust-scattering halo) and the distinctly bluer PSF, as can be seen from the color image in Figure 3. The two caps have very similar surface brightnesses ($\sim 2 \times 10^{-16}$ erg cm^{-2} s^{-1} arcsec^{-2}) and appear to be similar in their angular extent (NW: -5° – 65° ; SE: 185° – 245°). However, they are asymmetric in their radial extent (NW: $\sim 22''$ – $50''$, SE: ~ 18 – $45''$). The inner NW jet emission (Section 3.2) has similar position and opening angles to the NW cap.

The correspondence between the high-resolution radio contours ($\geq 2\sigma$) and the X-ray cap emission in Figure 2 is striking. While the X-ray image has significantly higher angular resolution than the radio, it is clear that the X-ray caps align closely with the extended jet emission.

The diffuse emission to the SE of the XRB in the radio image shows a sharp surface brightness drop at the position of the cap and what has been interpreted as a bend in the jet direction at this position, trailing to the south (referred to as “knot B” in Tudose et al. 2006). We see no clear corresponding surface brightness enhancement to this trail in the X-rays. However, our sensitivity is compromised by the fact that the read streak runs right along this feature.

We used partial annuli regions to extract the cap spectra. Because the background is dominated by the dust-scattering halo, the surface brightness of which depends on the angular distance to Circinus X-1, we carefully selected background partial annuli at the same radial extent as the source regions. We recover a total of 6240 source counts over 2860 expected background counts in both cap regions combined (0.5–9.5 keV). The resulting spectra are shown in Figure 4.

Initial extractions of each of the caps indicated that the spectral parameters are statistically indistinguishable. Therefore, we jointly fit the spectra. We restricted our spectral analysis to 0.5–9.5 keV. Quoted uncertainties correspond to 90% confidence intervals. The spectra are well fit by an absorbed powerlaw with a neutral hydrogen column of $N_{\text{H}} = 2.24_{-0.28}^{+0.30} \times 10^{22}$ cm^{-2} and a photon index, $\Gamma = 1.99_{-0.21}^{+0.23}$ ($\chi^2 = 243.1$ over 252 degrees of freedom), giving 0.5–9.5 keV cap fluxes of 3.2×10^{-13} erg cm^{-2} s^{-1} (NW) and 2.7×10^{-13} erg cm^{-2} s^{-1} (SE).

The caps can also be fit by a thermal (APEC) model ($\chi^2 = 237.7$ over 251 degrees of freedom). The required absorbing column is very similar to the power-law case

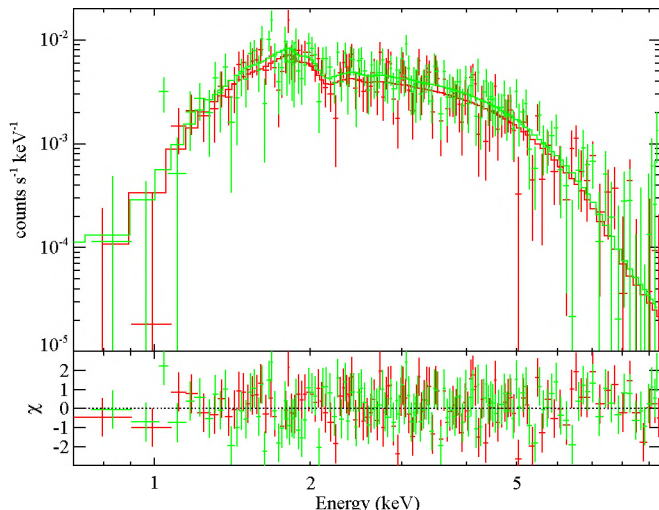


FIG. 4.— Top: spectrum of the two large-scale caps and best-fit absorbed power-law fit (red: NW cap; green: SE cap). Bottom: deviations from the best-fit model.

with $N_{\text{H}} = 1.93^{+0.21}_{-0.18} \times 10^{22} \text{ cm}^{-2}$. This is consistent with the fact that there is no obvious line emission present in the spectra, the APEC fit requires a low abundance of $Z = 0.41^{+0.38}_{-0.27}$ and a high temperature of $kT = 6.6^{+2.2}_{-1.8} \text{ keV}$. When forced to solar abundance, the fit requires even higher temperatures. The 0.5–9.5 keV cap fluxes are $3.2 \times 10^{-13} \text{ erg cm}^{-2} \text{ s}^{-1}$ (NW) and $2.7 \times 10^{-13} \text{ erg cm}^{-2} \text{ s}^{-1}$ (SE).

4. DISCUSSION

The limb-brightened morphology of the X-ray image (which has significantly higher angular resolution than either radio image) suggests that the emission from the two caps originates at a shock in the outflow from Circinus X-1, seen in projection. This suggestion is supported by a sharp drop in surface brightness in radio and X-ray just outside of the caps and by the fact that the SE radio jet seems to be changing direction at the location of the X-ray cap. The fact that the caps appear inside the large-scale radio nebula would be a result of foreshortening, since the jet axis is likely inclined with respect to the line of sight (though the actual inclination is unknown). The outflow itself appears largely X-ray dark (except for the inner NW diffuse radio–X-ray feature), similar to the X-ray cavities observed in many clusters with central radio galaxies.

The caps span projected half-opening angles of 35° (NW) and 30° (SE). This implies that either:

1. the outflow is, in fact, much wider than what would typically be considered a jet and might thus be better characterized as a non-thermal wind, or
2. the jets are precessing with a fairly wide opening angle, as is the case for SS433 (Margon 1984), and/or
3. the jet or precession cone axis is very close to the line of sight, causing significant foreshortening of an intrinsically narrow jet.

The wide opening angle of the *inner* NW jet would be consistent with (1) and (3), but to be consistent with (2), it would require a precession period of the jet that is short

compared to the travel time through the X-ray emission region to blend the jet emission (as seen in the arcsecond radio jets of SS433 Hjellming & Johnston 1981).

The claim of a highly relativistic jet ($\Gamma_{\text{jet}} \sim 16$, $\theta \lesssim 5^\circ$; Fender et al. 2004) coupled with these new observations would require that such a jet has a precession cone that is within 5° of the line-of-sight such that the jet sometimes points very close to the line-of-sight. Such a geometry would imply a physical scale of $\sim 20 \text{ pc}$ from cap to cap. For comparison, this is an order of magnitude larger than the projected distance between the hotspots of XTE J1550–564 (Corbel et al. 2002) and H1743–322 (Corbel et al. 2005) but would still fit comfortably within the radio nebula surrounding SS433 (Dubner et al. 1998).

Below, we will discuss two possible interpretations of the radiative origin of the cap emission.

4.1. Cooled Synchrotron Model

The most likely interpretation of the spectra is synchrotron emission. In this case, the emission arises from the reaccelerated jet particles entering the terminal shock, as is observed in the hot spots of many FR II radio galaxies (e.g., Meisenheimer et al. 1989). The X-ray emission in this case should be co-spatial with the radio, which appears consistent with the radio contours in Figure 2.

The radio synchrotron spectrum of the large-scale nebula has a typical spectral index of $\alpha_{\text{R}} = 0.53$ (with $F_{\nu} \propto \nu^{-\alpha_{\text{R}}}$) (Tudose et al. 2006), consistent with the standard power-law slope of first-order Fermi acceleration. For the canonical model of continuously injected power-law electrons one would expect a spectral index of $\alpha_{\text{X}} = \alpha_{\text{R}} + 0.53 = 1.03$ above the cooling break at frequency ν_{b} , perfectly consistent with the observed X-ray spectral index of $\alpha_{\text{X}} = 0.99$. From extrapolation of the radio and X-ray spectra, we estimate the break frequency from uncooled to cooled synchrotron emission to be $\nu_{\text{b}} \sim 2 \times 10^{16} \text{ Hz}$, which is uncertain by about an order of magnitude when uncertainties in the radio and X-ray spectral indices are used primarily because the X-ray and radio power-law slopes are extrapolated over a very large range of frequencies.

Taking the emission regions to be spherical to lowest order, we estimate the equipartition magnetic field strength to be $B_{\text{eq}} \sim 50 \mu\text{G}$, which gives a *minimum* total internal energy for each emission region of $\sim 8 \times 10^{45} \text{ erg}$. From the estimate of the break frequency, we estimate a cooling time, $\tau_{\text{cool}} \sim 1600 \text{ yr}$. A different emission geometry will change these numbers by factors of order unity.

Together, these numbers provide a robust *lower* limit on the total jet power of $P_{\text{cir}} > 3 \times 10^{35} \text{ erg s}^{-1}$, needed *just* to put the synchrotron emitting particles in place (not including any plasma currently in the jet or the energy needed to inflate the large-scale radio nebula). Departing from equipartition can only *increase* this number. This limit is *independent* of the assumed geometry and size of the emission regions.

Conversely, we can place a rough *upper* limit on the outflow power from the fact that the large-scale radio nebula must be at least as old as τ_{cool} . Using the same arguments as presented in Heinz (2002) and Tudose et al. (2006) for the expansion of the radio nebula we find that

$P_{\text{cir}} \lesssim 2 \times 10^{37} \text{ erg s}^{-1}$, though this limit is not as robust since the magnetic field could well be out of equipartition and the nebula could be significantly elongated along the line-of-sight, both of which would increase the total power.

These limits on P_{cir} confirm that the accreting compact object in this system is driving powerful jets into the interstellar medium (ISM). Taking the high 42 year average luminosity of Circinus X-1 at about 80% of the Eddington luminosity for a $1.4 M_{\odot}$ neutron star (Parkinson et al. 2003) at face value would imply that the long-term average jet power is between 2% and 10% of the *current* average radiative power.

Given that the average long-term accretion rate cannot greatly exceed the Eddington rate, we can derive a robust lower limit on the efficiency with which accretion power is converted into outflow power of $\eta_{\text{jet}} = P_{\text{cir}}/\dot{m}c^2 > 0.034\% \frac{\dot{m}_{\text{Edd}}}{\dot{m}}$ (see also Heinz et al. 2007 and Soleri et al. 2009).

4.2. Thermal Model

Given the equally good fit we achieved with a thermal emission model, it is worth discussing the alternative scenario that the X-ray caps are the shocked ISM pushed ahead of the expanding radio outflow (similar to the shells around many X-ray cavities in galaxy clusters and around the microquasar Cygnus X-1; Gallo et al. 2005).

In the thermal model the X-rays should be located further out from the binary than the radio emission. However, the high-resolution radio data indicate that the radio and the X-ray emission are co-spatial. This requires a very low inclination angle in order to align the two regions by projection (which is consistent with the inclination required by the ultra-relativistic flow claimed in Fender et al. 2004).

From the best-fit temperature of 6.6 keV, we directly

infer a shock velocity of $\sim 2.4 \times 10^3 \text{ km s}^{-1}$. From the projected distance, we can infer an estimated travel time of $\sim 500/\sin(\theta)$ years out to the observed shock positions for each of the caps. Again approximating the emission region as spherical, we estimate the mass and the total (thermal plus kinetic) energy of the shocked material for each of the caps to be $\sim 2 \times 10^{32} \text{ g}$ and $\sim 2 \times 10^{49} \text{ erg}$, respectively. Combined with the shock travel age, this gives a minimum outflow power for both caps combined of $P_{\text{cir}} > 6 \times 10^{38} \times \sin(\theta) \text{ erg}^{-1} \text{ s}^{-1}$, *just* to supply the X-ray emitting material (not including the putative power required to inflate the large-scale radio nebula). Unless the inclination angle is very small, this power is exceedingly large. Even for inclinations as low as those inferred from the relativistic jet claimed in Fender et al. (2004), the *minimum* average power would still be $P_{\text{cir}} > 5 \times 10^{37} \text{ erg s}^{-1}$.

While we cannot completely rule out a thermal origin, the very high power required by the thermal model combined with the perfect spectral correspondence to a classic broken synchrotron spectrum and the spatial correspondence with the radio suggest that the synchrotron model is the more natural choice.

5. SUMMARY

We have presented an initial analysis of a deep *Chandra* imaging observation of Circinus X-1. We detect two diffuse X-ray caps that are likely the terminal shocks of powerful jets running into the ISM. In addition, we find an arcsecond-scale outflow between the XRB and one of the X-ray caps, coincident with the radio jet. These discoveries make Circinus X-1 the first microquasar with both an X-ray jet and two stationary X-ray shocks, and one of only a handful of microquasars with a direct estimate of the jet power.

S.H. and P.S. acknowledge support from NASA grant GO9-0056X.

REFERENCES

- Brandt, W. N. & Schulz, N. S. 2000, ApJ, 544, L123
 Broos, P. S., Townsley, L. K., Feigelson, E. D., Getman, K. V., Bauer, F. E., & Garmire, G. P. 2010, ApJ, 714, 1582
 Corbel, S., Fender, R. P., Tzioumis, A. K., Tomsick, J. A., Orosz, J. A., Miller, J. M., Wijnands, R., & Kaaret, P. 2002, Science, 298, 196
 Corbel, S., Kaaret, P., Fender, R. P., Tzioumis, A. K., Tomsick, J. A., & Orosz, J. A. 2005, ApJ, 632, 504
 Dubner, G. M., Holdaway, M., Goss, W. M., & Mirabel, I. F. 1998, AJ, 116, 1842
 Fender, R., Wu, K., Johnston, H., Tzioumis, T., Jonker, P., Spencer, R., & van der Klis, M. 2004, Nature, 427, 222
 Gallo, E., Fender, R., Kaiser, C., Russell, D., Morganti, R., Oosterloo, T., & Heinz, S. 2005, Nature, 436, 819
 Heinz, S. 2002, A&A, 388, L40
 Heinz, S., Schulz, N. S., Brandt, W. N., & Galloway, D. K. 2007, ApJ, 663, L93
 Hjellming, R. M. & Johnston, K. J. 1981, ApJ, 246, L141
 Iaria, R., Spanò, M., Di Salvo, T., Robba, N. R., Burderi, L., Fender, R., van der Klis, M., & Frontera, F. 2005, ApJ, 619, 503
 Iaria, R., D’Aí, A., Lavagetto, G., Di Salvo, T., Robba, N. R., & Burderi, L. 2008, ApJ, 673, 1033
 Jonker, P. G., Nelemans, G., & Bassa, C. G. 2007, MNRAS, 374, 999
 Linares, M., et al. 2010, ATel, 2653, 1
 Lopez, L. A., Marshall, H. L., Canizares, C. R., Schulz, N. S., & Kane, J. F. 2006, ApJ, 650, 338
 Margon, B. 1984, ARA&A, 22, 507
 Meisenheimer, K., Roser, H., Hiltner, P. R., Yates, M. G., Longair, M. S., Chini, R., & Perley, R. A. 1989, A&A, 219, 63
 Parkinson, P. M. S., et al. 2003, ApJ, 595, 333
 Sault, R. J., Teuben, P. J., & Wright, M. C. H. 1995, in ASP Conf. Ser. 77, Astronomical Data Analysis Software and Systems IV, ed. R. A. Shaw, H. E. Payne, & J. J. E. Hayes (San Francisco, CA: ASP) 433
 Schulz, N. S. & Brandt, W. N. 2002, ApJ, 572, 971
 Schulz, N. S., Kallman, T. E., Galloway, D. K., & Brandt, W. N. 2008, ApJ, 672, 1091
 Soleri, P., et al. 2009, MNRAS, 397, L1
 Stewart, R. T., Caswell, J. L., Haynes, R. F., & Nelson, G. J. 1993, MNRAS, 261, 593
 Tennant, A. F., Fabian, A. C., & Shafer, R. A. 1986, MNRAS, 221, 27P
 Tudose, V., Fender, R. P., Kaiser, C. R., Tzioumis, A. K., van der Klis, M., & Spencer, R. E. 2006, MNRAS, 372, 417
 Tudose, V., Fender, R. P., Tzioumis, A. K., Spencer, R. E., & van der Klis, M. 2008, MNRAS, 390, 447